

RSC Advances

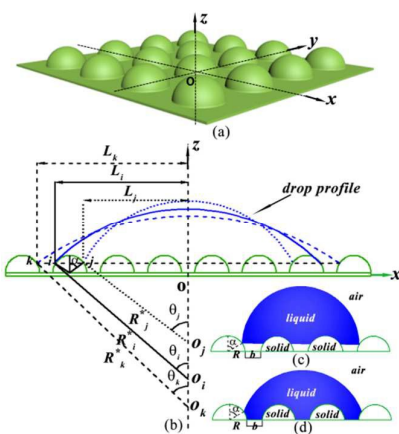


This is an *Accepted Manuscript*, which has been through the Royal Society of Chemistry peer review process and has been accepted for publication.

Accepted Manuscripts are published online shortly after acceptance, before technical editing, formatting and proof reading. Using this free service, authors can make their results available to the community, in citable form, before we publish the edited article. This *Accepted Manuscript* will be replaced by the edited, formatted and paginated article as soon as this is available.

You can find more information about *Accepted Manuscripts* in the [Information for Authors](#).

Please note that technical editing may introduce minor changes to the text and/or graphics, which may alter content. The journal's standard [Terms & Conditions](#) and the [Ethical guidelines](#) still apply. In no event shall the Royal Society of Chemistry be held responsible for any errors or omissions in this *Accepted Manuscript* or any consequences arising from the use of any information it contains.



Based on the thermodynamic analysis, the effects of chemistry and all the geometrical parameters for the semicircular microtexture on free energy and free energy barrier as well as equilibrium contact angle and contact angle hysteresis were theoretically discussed.

ARTICLE

Optimal Design of Superhydrophobic Surfaces Using a Semicircular Protrusion Microtexture

Cite this: DOI: 10.1039/x0xx00000x

Lu Tie^a, Zhiguang Guo^{a, b*}, W. Li^{c*}Received 00th January 2014,
Accepted 00th January 2014

DOI: 10.1039/x0xx00000x

www.rsc.org/

Superhydrophobic surfaces have shown promising applications in self-cleaning, anti-dust or icing, and anti-friction or wear. To fabricate such surfaces and achieve the best superhydrophobicity, the criterion to design surface geometry has been proposed. In this article, based on the thermodynamic analysis, the effects of chemistry (intrinsic CAs) and all the geometrical parameters for the semicircular microtexture on free energy (FE) and free energy barrier (FEB) as well as equilibrium contact angle (ECA) and contact angle hysteresis (CAH) have been theoretically investigated. It is demonstrated that semicircular base radius and intrinsic CA play a significant important role in ECA and CAH; in particular, a critical intrinsic CA and semicircle radius for the semicircular microtexture are necessary for the transition from non-composite to composite states. Furthermore, it is revealed that semicircle base spacing affect superhydrophobic behavior. Moreover, it is revealed that effect of outer vibrational energy on wetting behavior depend strongly on the surface texture and chemistry (intrinsic CAs). Based on the above effects, a criterion for the transition from non-composite to composite wetting states can be further obtained.

1. INTRODUCTION

Superhydrophobic surfaces with a unique wettability usually possess a very high contact angle (typically greater than 150°) and a very small contact angle hysteresis (the difference between advancing angle and receding contact angles, typically smaller than 10°). Such surfaces have attracted significant attentions within the scientific community during the past decades because of their excellent self-cleaning properties and their potential applications such as drug delivery¹, self-cleaning window glasses², solar panels³, antifouling⁴, micro-channels⁵ and so on.

For fabricating a superhydrophobic surface, there are two dominant approaches which combine surface chemistry and morphology, i.e., modifying low surface energy hydrophobic material on the rough surface and enhancing surface roughness in the low surface energy hydrophobic materials (intrinsic CA is greater than 90°)⁶. Because the maximum intrinsic CA of

^a State Key Laboratory of Solid Lubrication, Lanzhou Institute of Chemical Physics, Chinese Academy of Sciences, Lanzhou 730000, China.

^b Hubei Collaborative Innovation Centre for Advanced Organic Chemical Materials and Ministry of Education Key Laboratory for the Green preparation and Application of Functional Materials, Hubei University, Wuhan 430062, China.

^c Hubei Polytechnic University, Huangshi 435003, China.

E-mail: zguo@licp.cas.cn (GUO); wenzl@ualberta.ca (LI)

low surface energy hydrophobic material is 120°,⁷ while under extremely special circumstances and geometries, enhancing surface roughness in the low surface energy hydrophobic materials may lead to almost the maximum CA, i. e., 180°.⁸ As a result, various rough geometry to prepare superhydrophobic surface through different smart physical and chemical methods have been constructed.⁹⁻¹³ It is now becoming possible to control and tailor micro or nano-scale chemical structures with different geometrical patterns on various substrates to achieve so-called superhydrophobic surfaces.^{13, 14}

In spite of significant advances in preparation of such surfaces, to date the effects of surface patterns or geometries on superhydrophobicity have not been understood completely. In particular, in the theoretical aspect, such as CAH and wetting state transition (e.g., from non-composite to composite state). It has therefore been a challenge to design optimal geometry for ideal superhydrophobic behavior. In the recent years, considerable theoretical efforts have been made during the recent years. For example, to design optimal superhydrophobic surfaces, Quere et al.¹⁵ proposed a criterion of asperity ratio for the formation of a stable Cassie state. Extrand^{16,17} investigated effects of pillar height and base angle on the superhydrophobic behavior for a surface with hexagonal arrays of square asperities and further proposed a criterion contact line density criterion and asperity height criterion for the suspension and

collapse of a droplet on the surface. Patankar¹⁸ analyzed the wetting state transition for a periodical pillar microtextured surface and emphasized the effect of the ratio between pillar height and width on transition. In addition, Nosonovsky and Bhushan¹⁹ stressed the role of aspect ratio and meniscus force for different rough surfaces and further designed the optimal microtextured surfaces with hemispherical topped cylindrical and pyramidal asperities. The above studies have succeeded in the establishments of a quantitative correlation between different microtextured geometries and superhydrophobicity and are in agreement with specific experimental observations.

Recently, Li and Amirfazli^{20, 21} proposed a simple and robust thermodynamic approach for successful analysis of free energy (FE) and free energy barrier (FEB) of a metastable energy state. This approach is based on a two-dimension model, but it can offer a concise physical picture of energy status and hence can simplify calculations of CA and CAH associated with FE and FEB. Unfortunately, the model is mainly discussed on the pillar microtexture surface. The pillar microtexture surface is just the idealized model, which is different from the actual surface structure.

In this article, based on the proposed a thermodynamic approach to analyze FE and FEB of a metastable wetting state^{20, 21}, we extend the analysis to a more general surface structure, semicircular protrusions microtexture, as illustrated in Figure 1(c) and (d). In nature, lotus leaf has the similar paraboloid micro-structure surface. There are some advantages for the lotus leaf, such as self-cleaning and antifouling property. Nowadays, artificial methods for preparation paraboloid micro-structure surface are relatively less. Recently, the non-flatted top of paraboloid micro-structure surface is fabricated by the femtosecond laser irradiation method^{22,23}. In particular, compared to the previous pillar microtexture structure surface, semicircular microtexture has some advantages. First, it should be indicated that the semicircular microtexture hardly involves shape edges and corners, and hence can be fabricated using the practical micro- or nano-techniques. Meanwhile, it is difficult to erosion and breakage. Thus, semicircular microtexture possesses excellent mechanical properties. Second, semicircular microtexture is similar to the actual microtexture (e.g., for lotus microtexture). Third, compared to the previous work, the present study focuses on the essential role of intrinsic CAs and radius in the semicircular protrusions microtexture, which has been experimentally emphasized. Further, external means (vibrational energy) in determining wetting behaviours are investigated. The present study aims mainly at a deep insight into some guidelines for the optimal geometrical design of economical practical superhydrophobic surfaces and prediction of superhydrophobic behaviour. We hope that our study will stimulate further experimental investigate in this direction.

2. THERMODYNAMIC ANALYSIS

2.1. General Theoretical Considerations on a Semicircular Microtexture Surface

In principle, based on minimizing free energy (FE) of a system formed between a 3-dimensional surface structure and a drop, thermodynamically stable (equilibrium) and metastable states can be found. The key issue is to devise a simple analysis of a system and its boundary conditions to find metastable states of the system; to this end, this approach proposes that a 3-dimensional semicircular structure illustrated in Fig. 1(a) can be simplified into a 2-dimensional system by analyzing the system along specific planes such as $y = 0$, as illustrated in Fig. 1(b). Based on this simplification, the analysis of thermodynamic status related to surface geometrical configurations of the system and subsequent numerical calculation of FE barrier can be readily conducted. A point to note is that the methodology suggested here will not be applicable for nonsymmetric drops (such systems are not very

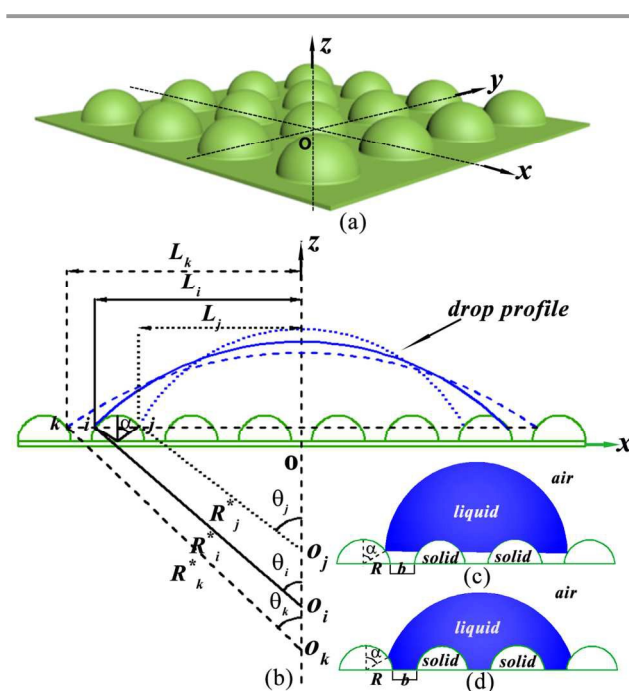


FIG. 1: (a) An enlarged view of a typical 3-D semicircular surface microtexture; (b) Illustration of variation of composite wetting states for a droplet from state i to j (or to k) shown in Fig (a) along the $y = 0$ plane. The inset shows a typical 2-D semicircular microtexture: (c) composite; (d) non-composite

common in practical cases).

It is well known that, the CA of a water droplet on an ideal smooth solid surface can be given by the classical Young's Equation

$$\gamma^{la} \cos \theta_Y = \gamma^{sa} - \gamma^{ls} \quad (1)$$

where θ_Y is intrinsic CA. γ^{la} , γ^{sa} , and γ^{ls} are the surface tension at liquid-air, solid-air, and liquid-solid interfaces, respectively. For a rough surface, there are two wetting states, which are the non-composite state (i.e., complete liquid penetration into the troughs of a roughness surface) and composite state (i.e., the

entrapment of air in the troughs of a roughness surface). Figure 1(c) and (d) show a semicircular protrusions microtextured surface and the two wetting states. Note that the surface microtexture is uniformly constructed from the constant geometrical parameters of semicircle base angle (α), radius (R) and space (b).

The apparent contact angle (θ_W) of non-composite state is given by Wenzel's Equation²⁴:

$$\cos \theta_W = r \cos \theta_Y \quad (2)$$

a roughness factor r can be defined (see Figure 1(d)):

$$r = \frac{\pi R + b}{2R + b} \quad (3)$$

For the composite wetting state, droplets are supported by a composite surface composed of solid and air, the apparent contact angle (θ_{CB}) can be given by Cassie Equation²⁵:

$$\cos \theta_{CB} = r_f f \cos \theta_Y + f - 1 \quad (4)$$

roughness ratio of the wet area r_f and the solid fraction f for the 2-D model may be represented as (see Figure 1 (c)):

$$r_f = \frac{\alpha}{\sin \alpha} \quad (5)$$

$$f = \frac{2R \sin \alpha}{2R + b} \quad (6)$$

One can expect that the free energy and free energy barrier should be modified by the parameters of semicircular base angle, radius and base spacing both non-composite and composite wetting state.

2.2. Thermodynamic Analysis for the Semicircular Protrusions Micro-textured Surface

In this article, on the basis of the proposed thermodynamic analysis, we extend the model and similar methodology to the semicircular protrusions micro-textured surfaces with a set of geometrical parameters (Figure 1(c) and (d)). Some assumptions have been made as before²⁰. FE and FEB associated with CA and CAH for non-composite and composite states can be numerically calculated. The following results can be obtained. For a non-composite state, if the droplet recedes from position i (with a CA of θ_i and droplet size of L_i) to j (with a CA of θ_j and droplet size of L_j), the geometrical relationship parameters (θ_i , R , b) can be written as:

$$\begin{aligned} & \theta_i \frac{L_i^2}{\sin^2 \theta_i} - L_i^2 \cot \theta_i - (\alpha R^2 - R^2 \sin \alpha \cos \alpha) \\ & = \theta_j \frac{L_j^2}{\sin^2 \theta_j} - L_j^2 \cot \theta_j \end{aligned} \quad (7)$$

The relative FE barrier for transition from i to j can be express as:

$$\frac{\Delta F_{i \rightarrow j}}{\gamma^{la}} = \theta_j \frac{L_j}{\sin \theta_j} - \theta_i \frac{L_i}{\sin \theta_i} + 2R\alpha \cos \theta_Y \quad (8)$$

Similarly, if the droplet advances from i to k (see Figure 1), one can obtain the geometrical relationship and the relative FE barrier for the transition, respectively.

$$\begin{aligned} & \theta_i \frac{L_i^2}{\sin^2 \theta_i} - L_i^2 \cot \theta_i^2 = \\ & \theta_k \frac{L_k^2}{\sin^2 \theta_k} - L_k^2 \cot \theta_k^2 + [(b + 2R) - R \sin \alpha] R \cos \alpha - R^2 \left(\frac{\pi}{2} - \alpha \right) \end{aligned} \quad (9)$$

$$\frac{\Delta F_{i \rightarrow k}}{\gamma^{la}} = \theta_k \frac{L_k}{\sin \theta_k} - \theta_i \frac{L_i}{\sin \theta_i} - [b + 2R \left(\frac{\pi}{2} - \alpha \right)] \cos \theta_Y \quad (10)$$

For a composite state (see Figure 1(b)), if the droplet recedes from position i to j , the geometrical relationship and the relative FE barrier for transition can be same as the noncomposite state, if the droplet recedes from position I to k , the geometrical relationship and the relative FE barrier for transition can be written as:

$$\theta_i \frac{L_i^2}{\sin^2 \theta_i} - L_i^2 \cot \theta_i^2 = \theta_k \frac{L_k^2}{\sin^2 \theta_k} - L_k^2 \cot \theta_k^2 \quad (11)$$

$$\frac{\Delta F_{i \rightarrow k}}{\gamma^{la}} = \theta_k \frac{L_k}{\sin \theta_k} - \theta_i \frac{L_i}{\sin \theta_i} + b + 2R(1 - \sin \alpha) \quad (12)$$

For the two-dimensional surface profile of semicircular protrusions, combining Eqs (5) and (6), the following condition must be met for a local extreme, as long as $\pi/2 < \theta_Y < \pi$, only if^{26, 27}

$$\alpha = \pi - \theta_Y \quad (13)$$

and

$$\frac{d^2(r_f f)}{df^2} = \frac{\sin \alpha}{\cos^3 \alpha} > 0 \quad (14)$$

Thus, a local minimum in free energy may exist at $\alpha = \pi - \theta_Y$. From the above analysis we can find that not all values of α between 0 and π are possible. The boundary conditions of constant volume and constant θ_Y limit $\alpha = \pi - \theta_Y$. That is, for each semicircular protrusion there are two metastable states positions. The above result indicates that the position of the droplet on semicircular protrusion is closely related to the intrinsic CAs for the composite wetting state, and a smaller amount of liquid penetration into the semicircular microtextured surfaces with increasing intrinsic CAs for hydrophobic material, which is different from the pillar microtexture.

Combining Eqs (7) - (14), the FE and FEB curves can be

obtained. We give a typical example to show how to get various CA and contact angle hysteresis (CAH) from the analysis and calculations of FE and FEB. Figure 2(a) illustrates two FE curves. It is clear that there is only one point of the lowest FE for each curve which is associated with the equilibrium CA (ECA). However, if CA changes slightly on the order of 10^{-3} degree (e.g., droplet recedes from a position i to j or advances from i to k), the local curve can show a fluctuation in FE, as illustrated in the inset of Figure 2(a). These fluctuations demonstrate that the FE curve contains multivalued local minimum FE and maximum FE, indicating that such extremes represent metastable and unstable equilibrium states, which are

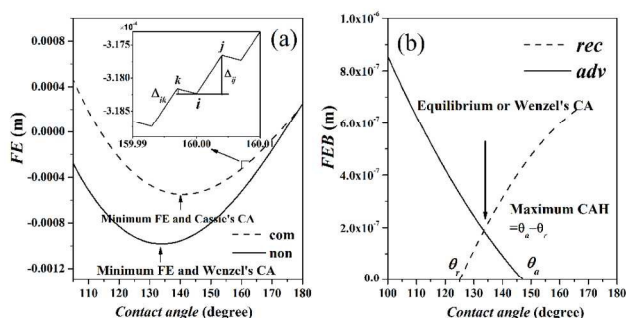


FIG. 2: (a) Variation of normalized FE with CA for a non-composite (non) and composite (com) states. The inset shows an enlarge view of a segment of FE curve illustrating the FEB; positions i , j , and k correspond to those in Figure 1. Δ_{ij} and Δ_{jk} represent the FEB for retreating and advancing contact line, respectively; (b) Determining receding and advancing CAs as well as CAH from the typical curves of advancing and receding FEBs for a non-composite wetting state ($L = 0.01$ m, $b = 1$ μ m, $R = 1$ μ m; intrinsic CA, $\theta_v = 120^\circ$). The CAH shown is the maximum value associated with zero FEB on the advancing and receding branches of the FE curve.

related to various apparent CAs. Therefore, the FEB refers to the difference between local minimum and maximum in the direction of three-phase line motion, i.e., advancing and receding. Furthermore, there are always two FEBs, i.e., advancing FEB and receding FEB, connected to each CA value (e.g., the advancing Δ_{ij} and receding Δ_{jk} along the three-phase line as illustrated in the inset of Figure 2(a)). Figure 2(b) shows the advancing and receding FEB for a non-composite state based on the same geometrical parameters as illustrated in Figure 2(a). The advancing CA (θ_a) and receding CA (θ_r) as well as CAH defined as $(\theta_a - \theta_r)$ can be determined by the intersecting values of advancing and receding curves with the x-axis, respectively. Here it is noted that for CAH, the theoretical treatments in the present model, where the liquid volume or area keeps unchanged but the droplet edge (three-phase contact line) advances or recedes to achieve the advanced or receded CA, are somewhat different from the experimental measurements, where the droplet edge (three-phase contact line) keeps stationary but the liquid volume or area increases or decreases to achieve the advanced or receded CA. Furthermore, the ECA can also be determined by the FEB curves, i.e., the intersecting point between advancing and receding curves in Figure 2(b). One can see that the value of ECA is consistent with the calculated value in Figure 2(a). Here it should be pointed out that the external energy, which was first termed by Johnson and Dettre, is assumed to have a value of zero.²⁸

2.3. The FE analysis for the transition from non-composite to composite wetting states

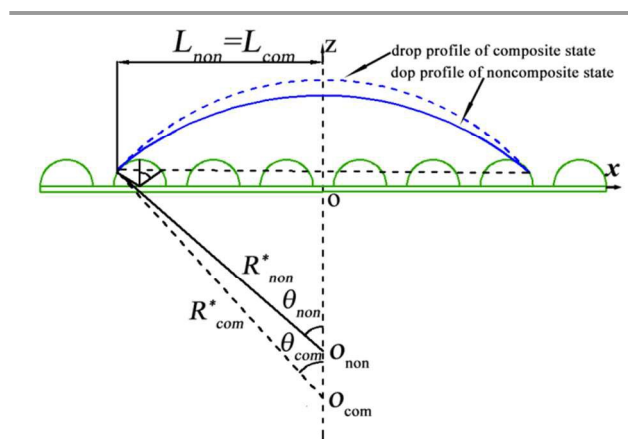


FIG. 3: Illustration of FE analysis for the transition between non-composite and composite states (note droplet volume is considered constant for both states)

Here, we derive the FE change for the transition from a non-composite to a composite state. Consider a non-composite state associated with a droplet width (L_{non}) and a CA (θ_{non}), as illustrated in Fig. 3. If such system exhibits a composite state associated with an equivalent droplet width ($L_{non} = L_{com}$) and a CA (θ_{com}), the FE per unit length of contact line, F , for these two states can be expressed as:

$$F_{non} = \gamma^{la} l_{non}^{la} + \gamma^{ls} l_{non}^{ls} + C \quad (15)$$

and

$$F_{com} = \gamma^{la} l_{com}^{la} + \gamma^{ls} l_{com}^{ls} + C \quad (16)$$

where C is the FE of the portion of the system that remains unchanged as a result of the transition between non-composite and composite states. Note that given the geometry of the system studied, the following relationships exist: $l_{non}^{la} = \theta_{non} L_{non} / \sin \theta_{non}$, $l_{non}^{ls} = L_{non} [b + 2R(\pi/2 - \alpha)] / (2R + b)$, $l_{com}^{la} = \theta_{com} L_{com} / \sin \theta_{com} + L_{com} [b + 2R - 2R \sin \alpha] / (2R + b)$, and $l_{com}^{ls} = L_{com} [b + 2R(\pi/2 - \alpha)] / (2R + b)$. Applying the constant droplet volume constraint or its 2D equivalent, constant droplet area in x - z plane allows derivation as:

$$\begin{aligned} & \theta_{non} \frac{L_{non}^2}{\sin^2 \theta_{non}} - L_{non}^2 \cot^2 \theta_{non} \\ & + \frac{L_{non}}{2R + b} [(b + 2R) - R \sin \alpha] R \cos \alpha - R^2 \left(\frac{\pi}{2} - \alpha \right) \\ & = \theta_{com} \frac{L_{com}^2}{\sin^2 \theta_{com}} - L_{com}^2 \cot^2 \theta_{com} \end{aligned} \quad (17)$$

Because Young's Equation is locally valid, the FE change for the transition from a non-composite state to a composite state can be expressed as:

$$\frac{\Delta F_{non \rightarrow com}}{\gamma^{la}} = \theta_{com} \frac{L_{com}}{\sin \theta_{com}} - \theta_{non} \frac{L_{non}}{\sin \theta_{non}} \quad (18)$$

$$- \frac{L_{com}}{2R+b} \left\{ (b+2R-2R \sin \alpha) + [b+2R(\frac{\pi}{2}-\alpha)] \cos \theta_Y \right\}$$

3. EFFECTS OF INTRINSIC CA

3.1. Effect of intrinsic CA on FE and ECA

In an ideal case, i.e., the outer vibrational energy equal zero. For applications of hydrophobic materials, in this section we discuss the effects of intrinsic CA larger than 90°. Variations of normalized free energy (FE) with respect to apparent CA for

sharply with increasing intrinsic CA for the non-composite state and exactly correspond to the Equation predicted by Wenzel or Cassie for the non-composite or composite state.

3.2. Effect of intrinsic CA on FEB, CAH and Wetting Transition

In an ideal case, i.e., the outer vibrational energy equal zero. Figure 4(c) shows the effect of intrinsic CA on the FEB for non-composite and composite wetting states. It is interesting to note that there is a critical intrinsic CA $\theta_Y = 120^\circ$, if θ_Y exceeds the critical value, the system will prefer the composite state, and the advancing CA (θ_a) keeps unchanged but the receding CA (θ_r) increases with intrinsic CA as free energy barrier equal zero. On the contrary, if θ_Y is lower than the critical value, the

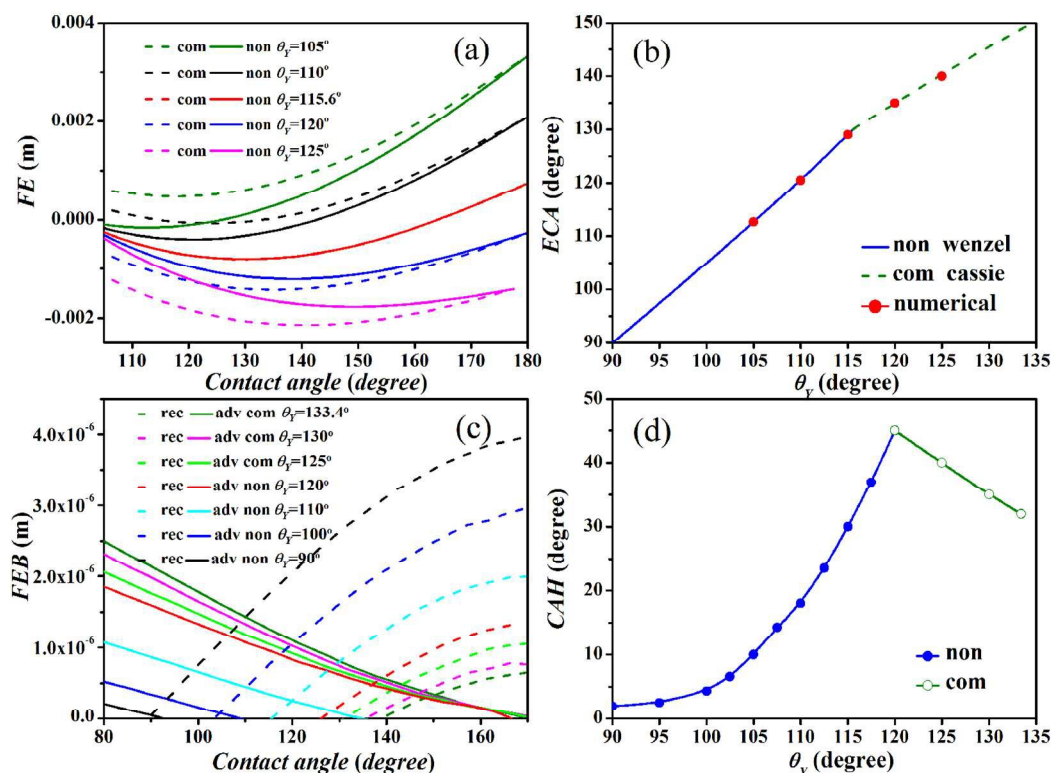


FIG. 4: (a) Variations of normalized FE against apparent CA for different intrinsic CA (θ_Y) with non-composite and composite wetting states; (b) Dependent of ECA against intrinsic CA with non-composite and composite wetting states ($L = 0.01$ m, $b = 1$ μ m, $R = 3$ μ m); (c) Variations of normalized FEB with respect to apparent CA for different intrinsic CA with non-composite (non) and composite (com) wetting states. (d) Thermodynamically plausible variations of CAH versus the intrinsic CAs for systems (adv and rec denote advancing and receding; non and com denote non-composite and composite $L = 0.01$ m, $b = 1$ μ m, $R = 2$ μ m).

the system with different intrinsic CA are shown in Fig. 4(a). It is important to note that the critical intrinsic CA values ($\theta_Y = 115.6^\circ$, i.e., the overlapped values for the non-composite and composite states) can be found. Note that if intrinsic CA exceeds the critical values, the FE curve of non-composite is higher than that of composite state. From a thermodynamic point of view, the composite state is more stable than the non-composite state; i.e., the system will prefer the composite state. However, if intrinsic CA is lower than the critical values, the system will prefer the non-composite state. Furthermore, the ECA with the lowest FE locus can be determined as shown in Figure 4(b). One can see that the calculated ECA increases

sharply with increasing intrinsic CA for the non-composite state, and the advancing CA and the receding CA increase with intrinsic CA as free energy barrier equal zero. One can also see that all the advancing FEB increase with increasing θ_Y , whereas the receding FEB decrease with increasing θ_Y both the non-composite and composite state.

It is well known that intrinsic CA is an important factor in determining the magnitude of the CAH. Based on the FEB curves, for an ideal case, i.e., the vibrational energy is zero; thermodynamically plausible variations of CAH versus the intrinsic CAs for systems with various semicircular base radius can be obtained, as illustrated in Fig. 4(d). It has been

demonstrated that a critical height is necessary to promote the transition from non-composite to composite states.^{16, 29, 30} However; the present results also reveal the essential effect of base angle for the transition. From Fig. 4(d), one can see that for the semicircular protrusions microtexture, a critical intrinsic CA is also necessary to guarantee the transition between the non-composite to composite states. Furthermore, on the basis of the above thermodynamic analysis, it can be found that the critical intrinsic CA ($(\theta_Y)_C$) can be obtained if both FE and FEB of the non-composite and composite states are equal. Therefore, a criterion for the transition can be expressed as

$$\theta_Y > (\theta_Y)_C \quad (19)$$

Here, it should be indicated that such an important role of base angle has also been stressed in the previous studies. For example, Marmur²⁷ theoretically analyzed the transition between Cassie and Wenzel states on roughness surfaces and found that the stable Cassie state can be formed only if $\alpha = \pi - \theta_Y$ for semicircular protrusions surface. It should be also noted that for a fixed semicircular base radius, droplet adhesion can be minimized for self-cleaning properties with smaller intrinsic

composite state. The above results indicate that intrinsic CA affects the transition between non-composite and composite states. Thus, for the design of superhydrophobic surfaces, a larger intrinsic CA is necessary to obtain high contact angle and low contact angle hysteresis.

4. EFFECTS OF SEMICIRCLE RADIUS (R) AND SPACE (b)

4.1. Effects of Semicircle Radius and Space on FE and ECA

Before the problem has been discussed, the parameter $\xi = R/b$ is defined; the parameter R stands for semicircle radius and b stands for the base space. In an ideal case, i.e., the outer vibrational energy equal zero. Dependents of normalized free energy (FE) against apparent CA for the system with different semicircle radius and space are shown in Figure 5(a). It is important to note that the critical semicircle radius values ($\xi_s = 2$, i.e., the overlapped value for both non-composite and composite states) can be found. It is interesting to note that for fixed semicircle space, if semicircle radius exceeds the critical value, the system will prefer the composite state. However, if semicircle radius is lower than the critical value, the system

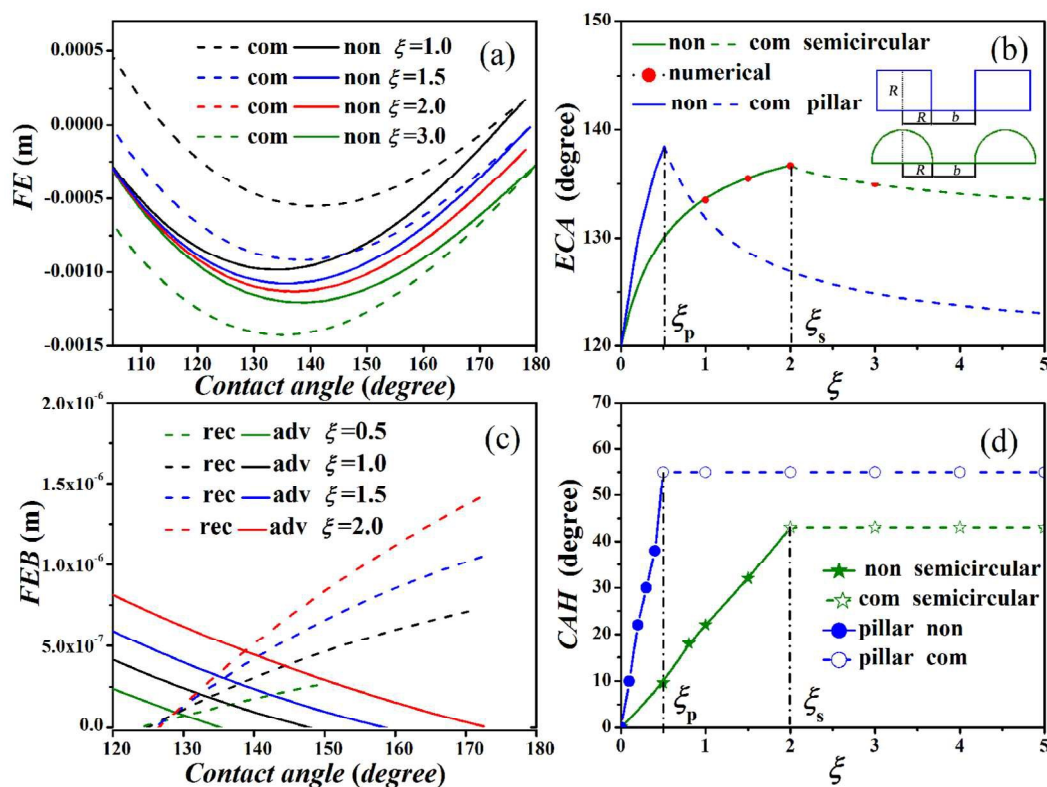


FIG. 5: (a) Dependent of normalized FE against apparent CA for different semicircle radius R and base space with non-composite and composite wetting states; (b) Dependent of ECA against semicircle radius (R) and space (b) for the pillar and semicircular microtexture system; (c) Variations of normalized free energy barrier (FEB) with respect to apparent CA for semicircle radius and space (b) for the pillar and semicircular systems (adv and rec denote advancing and receding; non and com denote non-composite and composite $L = 0.01$ m, $\theta_Y = 120^\circ$, $\xi = R/b$).

CAs in non-composite state or larger intrinsic CAs in will prefer the non-composite state. Meanwhile, for fixed the

semicircle radius, the situation is opposite; note that the composite state is more stable than non-composite state if base spacing is below a critical value. However, if base spacing is larger the critical value, the non-composite state is more stable. Further, the ECA depends on semicircle radius and spacing for both non-composite and composite states are shown in Fig. 5(b). For the non-composite state, the ECA increases with increasing semicircle radius or decreasing semicircle base spacing and exactly correspond to the Equation predicted by Wenzel. However, for the composite state, the ECA slightly decreases with increasing semicircle radius or decreasing semicircle base spacing and exactly correspond to the Equation predicted by Cassie. This result is also consistent with the experimental observation (e.g., Cao et al.³¹ found that Cassie CA decreased with decreasing spacing). The above results imply that the superhydrophobicity has been dramatically influenced by the geometrical parameters of semicircular for non-composite state, but the superhydrophobicity almost kept as constant for composite state.

4.2. Effects of Semicircle Radius and Space on FEB and CAH and Wetting Transition

In an ideal case, i.e., the outer vibrational energy equal zero. Figure 5(c) shows the effects of different semicircle radius and space on the FEB. For fixed the semicircle space, it is interesting to note that there is a critical semicircle radius. If R exceeds the critical value, the system will prefer the composite state, and the advancing and receding CA keeps unchanged with semicircle radius as free energy barrier equal zero. However, if R is lower than the critical value, the system will prefer the non-composite state. The receding CA (θ_r) keep unchanged but the advancing CA (θ_a) increases with increasing semicircle radius as free energy barrier equal zero. Based on the FEB curves, thermodynamically plausible variations of CAH versus the semicircle radius and spacing for systems can be obtained, as illustrated in Figure 5(d). One can see that for the semicircular protrusions microtexture, a critical semicircle radius is also necessary to guarantee the transition between the non-composites to composite states. It should be also noted that CAH is insensitive to the semicircle radius for the composite states. One can also see that all the advancing and receding FEB for both the non-composite and composite states increase with increasing R . On the contrary, the situation is opposite for fixed the base radius, one can see that the advancing FEB curves shift downward with increasing of base spacing and the receding FEB curves keep constant for the composite state; therefore, the resultant CAH of the composite state does not depend on semicircle base spacing as shown in Figure 5(d). For the non-composite state, the FEB for an advancing case changes, and the resultant CAH increases to the maximum value with decreasing of base spacing, whereas the receding FEB remains the same. In addition, from Figure 5(c) one can see that with decreasing base spacing the non-composite state transfers to the composite state and transition point corresponds to a critical base spacing. This indicates that small base spacing is needed for the transition. This result has also been supported

by relevant experimental observations. For example, Nakae et al.³² studied the effects of roughness pitch of surfaces on their wettability and found that narrow pitch (i.e., small spacing) can result in the transition. The above results indicate that semicircle radius and spacing affect the transition between non-composite and composite states. From the perspective of optimization design, we should try to choose the semicircle radius in the critical value for preparation hydrophobicity surface, since the superhydrophobicity is stronger in the critical value. However, the superhydrophobicity is unchanged with increasing semicircle radius. So over large semicircle radius is unnecessary, since for such microtexture, it is easy to wear and tear, leading to a poor mechanical property. Furthermore, a critical semicircle radius can also be obtained if both FE and FEB of the non-composite and composite states are equal. Therefore, a criterion for the transition can be expressed as:

$$\xi > \xi_c \quad (20)$$

On the transition point, we have $\theta_{non} = \theta_{com}$, Equation (18) is reduced to

$$\xi_c = \frac{1 + \cos \theta_Y}{2(\sin \theta_Y - 1) + (\pi - 2\theta_Y) \cos \theta_Y} \quad (21)$$

For an ideal case, i.e., the outer vibrational energy is zero, it is interesting to note that with increasing semicircle radius or decreasing intrinsic CA plays the equivalent role in the transition between non-composite and composite states.

Here it should be pointed out that compared to the previous theoretical model using a pillar microtexture, the present work indicates that the semicircle radius is relatively lower than the pillar height with higher base spacing under the same roughness factor. Therefore, for the future optimal geometrical design of an ideal superhydrophobic surface, one could avoid the use of the higher height pillar that should be prone to erosion and breakage³³. Furthermore, such a surface made of semispherical protrusions can emphasize the importance of at least two degrees of freedom in the geometric parameters, indicating a considerable convenience for the design of practical superhydrophobic surfaces. Moreover, the above calculations clearly show that the ECA or CAH relatively is larger or lower than the pillar structure under the same conditions as shown in Figure 5 (b) and (d). The pillar edge may pin a moving droplet and increase the CAH. Thus, based on a set of criteria, the semicircular protrusion microtexture for surface geometry can guarantee not only the stronger superhydrophobicity but also suitable mechanical characteristics. In addition, the present work can provide both thermodynamic and mechanistic explanation of how nature has developed a mechanically durable superhydrophobic surface, which can be a further inspiration for the design and fabrication of artificial surfaces.

5. EFFECTS OF OUTER VIBRATIONAL ENERGY

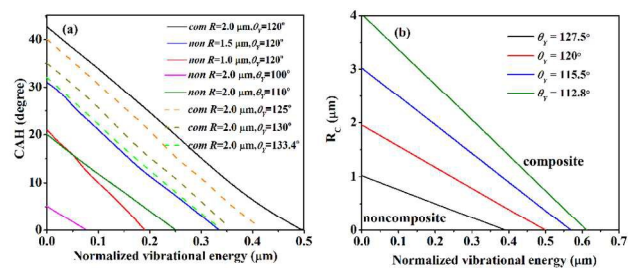


FIG. 6: (a) Variations of CAH for non-composite and composite state versus the normalized vibrational energy with different intrinsic CAs and semicircle radius ($L = 0.01$ m; $b = 1$ μm); (b) Variations of critical semicircle radius for the transition between non-composite and composite state versus the normalized vibrational energy with different intrinsic CAs ($L = 0.01$ m; $b = 1$ μm).

It is well known that the wetting properties are dramatically affected by environment vibration or additional energy such as temperature, light, sound vibration, static and other factors.^{34, 35} Johnson and Dettre²⁸ pointed out that vibration can provide additional energy with droplet to overcome the free energy. The vibration energy can be closely related to the dynamic contact angle of droplet (especially the contact angle hysteresis). Regardless of the physical nature of the vibrational energy, in the present study it is important to investigate how the vibrational energy affects CAH. Based on the FEB curves, the variations of CAH for non-composite states versus the normalized vibrational energy with different semicircle radius are shown in Figure 6(a). One can see that in general, CAH gradually tends to zero with increasing vibrational energy for different semicircle radius in non-composite states. This is consistent with the experimental results³⁶ for heterogeneous and/or rough surfaces. Further investigation shows that for a given vibrational energy level, the droplet adhesion can be decreased by reducing the semicircle radius in non-composite states. In case of the change in surface chemistry (intrinsic CA), the effects of the vibrational energy on CAH remains the same, i.e., with increasing vibrational energy, the CAH will decrease and eventually reach zero (see Figure 6(b)). It is interesting to note that, for a given vibrational energy level, the droplet adhesion for self-cleaning will be decreased with increasing the intrinsic CAs in the composite state or decreasing intrinsic CAs in non-composite state. However, to fully understand the physical nature of above findings, it seems that experimental studies^{31, 36} are inadequate. Compared Figure 6(a) with 6(b), it should be noted that under the same condition, the droplet with lower semicircle radius or intrinsic CA in a non-composite state is more easily roll. The above results demonstrate that the effect of outer vibrational energy on the wetting behavior is different, depending on the surface texture and chemistry (intrinsic CAs).

In fact, the wetting transition is dramatically affected by environment vibration or additional energy. If outer vibrational energy overtakes FEB for the transition from non-composite to composite state, droplet will overcome through the surface potential barrier and jump from non-composite to composite state. Thus, a complete understanding on why and how outer

vibrational energy affects the transition is essential for the design and prediction of superhydrophobic behavior. Especially, such understanding provides the basis for controlling superhydrophobic surface. Considering the outer vibrational energy, the criterion for the transition from non-composite to composite wetting states can be obtained. Based on Eq. (18), for the transition point, $\theta_{non} = \theta_{com}$, the critical condition for the transition between non-composite and composite states is

$$\Delta E = \frac{\Delta F_{non \rightarrow com}}{\gamma^{la}} = \frac{L_{com}}{2R+b} \{ (b+2R-2R \sin \alpha) + [b+2R(\frac{\pi}{2}-\alpha)] \cos \theta_Y \} \quad (22)$$

which results in the critical semicircle radius

$$R_C = \frac{\Delta E(b+2R) - Lb(1+\cos \theta_Y)}{2L(\sin \theta_Y - 1) + (\pi - 2\theta_Y)L \cos \theta_Y} \quad (23)$$

where ΔE is the outer vibrational energy. The critical semicircle radius R_C with respect to vibrational energy for the transition from non-composite to composite wetting states with different intrinsic CAs can be obtained, as illustrated in Fig. 6(b). It is interesting to note that, for a fixed the intrinsic CA, the critical semicircle radius R_C decreases with increasing vibrational energy, meanwhile, for a fixed the semicircle radius, the intrinsic CA decreases with increasing vibrational energy, indicating the transition from non-composite to composite wetting states with a lower semicircle radius or intrinsic CA will be obtained by increasing the out vibrational energy. The above results indicate the critical criteria for maintaining the composite wetting state are closely related to the outer vibrational energy and the surface texture dimension. Thus, the wetting behavior of semicircular microtexture surfaces can be manipulated by the outer vibrational energy and the surface texture dimension.

7. CONCLUSIONS

Based on the thermodynamic approach, we have theoretically investigated the superhydrophobic behavior for semicircular microtextured surfaces. Effects of chemistry and various geometrical parameters of the semicircular microtextured on FE and FEB as well as ECA and CAH are discussed in detail. It is demonstrated for the semicircular microtexture, intrinsic CA and semicircle radius play a significant important role in ECA and CAH; in particular, a critical intrinsic CA and semicircle radius for the present geometrical system, are necessary for the transition from non-composite to composite states. A criterion for judging such transition is therefore obtained. It is found that if intrinsic CA exceeds the corresponding critical value, the composite state is more stable and droplet adhesion can be minimized for self-cleaning properties with larger intrinsic CAs, however, the droplet adhesion almost keep unchanged with the semicircle radius (R). Comparatively, a small base space is necessary for the transition from non-composite to composite.

The calculation results are consistent with the experiment. In addition, it is revealed that the effects of outer vibrational energy on wetting behavior depend on the surface texture and chemistry (intrinsic CAs). Finally, based on a set of criteria, compare with the pillar microtexture, the semicircular protrusion microtexture for surface geometry can guarantee not only the stronger superhydrophobicity but also suitable mechanical characteristics.

Acknowledgments

This work is supported by the National Natural Science Foundation of China under Grant Nos. 11172301, and 21203217, and the Western Light Talent Culture project and the Top Hundred Talents project of Chinese Academy of Sciences.

Notes and references

- 1 S. T. Yohe, Y. L. Colson and M. W. Grinstaff, *J. Am. Chem. Soc.* 2012, **134**(4), 2016-2019.
- 2 Z. G. Guo, W. M. Liu and B. L. Su, *J. Colloid Interface Sci.*, 2011, **353**, 335-355.
- 3 H. Budunoglu, A. Yildirim, M. O. Guler and M. Bayindir, *ACS Appl. Mater. Interfaces*, 2011, **3**, 539-545.
- 4 M. Kobayashi, Y. Terayama, H. Yamaguchi, M. Terada, D. Murakami, *Langmuir*, 2012, **28**, 7212-7222.
- 5 C. H. Choi, U. Ulmanella, J. Kim, C. M. Ho and C. Kim, *J. Phy. Fluids.*, 2006, **18**, 087105.
- 6 (a) Z. G. Guo and W. M. Liu, *Plant Science*. 2007, **172**, 1103-1112. (b) G. Y. Wang, Z. G. Guo and W. M. Liu, *J. Bionic Eng.* 2014, **11**, 325-345. (c) B. Wang, W. X. Liang, Z. G. Guo and W. M. Liu, *Chem. Soc. Rev.* 2014, DOI: 10.1039/C4CS00220B. (d) S. Yu, Z. G. Guo and W. M. Liu, *Chem. Commun.* 2014, DOI: 10/1039/C4CC06868h. (e) H. Zhu, Z. G. Guo and W. M. Liu, *Chem. Commun.* 2014, **50**, 3900-3913.
- 7 T. Nishino, M. Meguro, K. Nakamae, M. Matsushita and Y. Ueda, *Langmuir*, 1999, **15**, 4321-4323.
- 8 (a) T. Y. Liu and C. J. Kim, *Science*. 2014, **346**, 1096-1100. (b) E. Hosono, S. Fujihara, I. Honma and H. Zhou, *J. Am. Chem. Soc.* 2005, **127**, 13458-13459.
- 9 H. Y. Erbil, A. L. Demirel, Y. Avc and O. Mert, *Science* 2003, **299**, 1377-1380.
- 10 Y. Xin, Z. G. Guo, *Chem. Lett.* 2014, **43**, 305-306.
- 11 (a) Z. G. Guo, F. Zhou, J. C. Hao, W. M. Liu, *J. Am. Chem. Soc.* 2005, **127**, 15670-15671. (b) Z. G. Guo, F. Zhou, J. C. Hao and W. M. Liu, *J Colloid Interface Sci*, 2006, **303**, 298-305.
- 12 Q. Xie, J. Xu, L. Feng, L. Jiang, W. Tang, X. Luo and C. C. Han, *Adv. Mater*, 2004, **16**, 302-305.
- 13 K. K. S. Lau, J. Bico, K. B. K. Teo, M. Chhowalla, G. A. J. Amaratunga, W. I. Milne, G. H. McKinley and K. K. Gleason, *Nano Lett*, 2003, **3**, 1701-1705.
- 14 V. Zorba, E. Stratakis, M. Barberoglou, E. Spanakis, P. Tzanetakis and C. Fotakis, *Appl. Phys. A: Mater. Sci.*, 2008, **93**, 819-825.
- 15 D. Quere, *Ann. Rev. Mater. Res.* 2008, **38**, 71-99.
- 16 C. W. Extrand, *Langmuir*, 2004, **20**, 5013-5018.
- 17 C. W. Extrand, *Langmuir*, 2002, **18**, 7991-7999.
- 18 N. A. Patankar, *Langmuir*, 2003, **19**, 1249-1253.
- 19 M. Nosonovsky and B. Bhushan, *Microsyst. Technol.*, 2005, **11**, 535-549.
- 20 W. Li and A. Amirfazli, *J. Colloid and Interface Sci.*, 2005, **292**, 195.
- 21 W. Li and A. Amirfazli, *Adv. Colloid Interface Sci.* 2007, **132**, 51.
- 22 A. M. Kietzig, S. G. Hatzikiriakos, P. Englezos, *Langmuir.*, 2009, **25** (8), 4821-4827.
- 23 S. Moradi, S. Kamal, P. Englezos, S. G. Hatzikiriakos, *Nanotechnology* 2013, **24**, 415302.
- 24 R. N. Wenzel, *Ind. Eng. Chem.*, 1936, **28**, 988-994.
- 25 A. B. D. Cassie and S. Baxter, *Trans. Faraday Soc.* 1944, **50**, 546551.
- 26 K. Rektorys, *K. Survey of Applicable Mathematics*, 2nd ed.; Kluwer Academic Publishers: Dor drecht/Boston/London, 1994.
- 27 A. Marmur, *Langmuir*, 2002, **18**, 8919.
- 28 R. E. Johnson and R. H. Dettre, *Advances in Chemistry Series*, 1964, **43**, 112-135.
- 29 N. A. Patankar, *Langmuir*, 2004, **20**, 7097-7102.
- 30 Z. Yoshimitsu, A. Nakajima, T. Watanabe and K. Hashimoto, *Langmuir*, 2002, **18**, 5818 -5822
- 31 L. Cao, H. H. Hu and D. Gao, *Langmuir*, 2007, **23**, 4310-4314.
- 32 H. Nakae, M. Yoshida and M. Yokota, *J. Mater. Sci.* 2005, **40**, 2287-2293.
- 33 Y. Yu, Z. H. Zhao and Q. S. Zheng, *Langmuir*, 2007, **23**, 8212.
- 34 E. L. Decker, S. Garoff, *Langmuir*, 1996, **12**, 2100.
- 35 V. C. Della, D. Maniglio, M. Morra and S. Siboni, *Colloids Surfaces A: Physicochem Eng Asp*, 2002, **206**, 47.
- 36 T. S. Meiron, A. Marmur and I. S. Saguy, *J Colloid Interface Sci*, 2004, **274**, 637.